15

Electrochemical Impedance Spectroscopy (EIS)

15.1 Introduction

The use of a phase-sensitive voltmeter for the study of the electrical response of the interphase can provide highly accurate measurements of the double-layer capacitance. However, this instrument has far more important uses in electrochemistry than just the measurement of capacitance. By combining a phase-sensitive voltmeter (also called a lock-in amplifier) with a variable frequency sine wave generator, one obtains an electrochemical impedance spectrometer. This makes it possible to probe the interphase over a wide range of frequencies and to record and analyze the data.

Electrochemical impedance spectroscopy (EIS) is an experimental AC technique that is based on the measurement of the complex impedance Z of an electrochemical system, which is either at steady state or at equilibrium. The impedance is measured as a function of the frequency f (Hertz, or cycles per second), or the angular frequency $\omega \equiv 2\pi f$ (rad s^{-1}), of an imposed sinusoidal perturbation of small amplitude. The amplitude of the applied potential is generally in the range of ± 5 to ± 25 mV at room temperature. The term "spectroscopy" stems from the use of frequency as a variable. Different processes at the surface of the electrode absorb electric energy at discrete frequencies, which causes time lag and measurable phase angle between the time-dependent excitation and the response signal. Such processes can be simulated with the aid of equivalent electrical circuits. The measurement is conducted within a large range of frequencies, say from millihertz to hundreds of kilohertz, or even microhertz to megahertz. The latter range of about 12 orders of magnitude is very high compared to other fields of spectroscopy. We recall, for instance, that visible light extends over a factor of just two in frequency. The range of frequencies that can be used in practice is limited by the electrochemical aspects of the system, not by instrumentation. Thus, measurements at very low frequencies take a long time, during which the interphase may change chemically. While it is technically possible to make measurements at, say, 10 μHz, this would take longer than a day to complete one cycle, and the changes in the interphase during the measurement at a single frequency could make the result meaningless. At the high-frequency end, stray capacitances and inductances combine with possible nonuniformity of current distribution at the electrode surface, to make the

Physical Electrochemistry: Fundamentals, Techniques, and Applications,
Second Edition. Noam Eliaz and Eliezer Gileadi.

results unreliable. For these reasons, it is recommended to limit measurements in the range of 10 mHz to 50 kHz, except when solid phases are tested.

The impedance of the system may be measured using various techniques, including frequency response analysis, phase-sensitive detection (PSD), and fast Fourier transform (FFT). Frequency response analyzers (FRAs) are instruments that determine the frequency response of a measured system. Their functioning is different from that of lock-in amplifiers. They are based on the correlation of the studied signal with the reference. The measured signal is multiplied by the sine and cosine of the reference signal of the same frequency and then integrated during one or more wave-periods. Such integration recovers the real and imaginary parts of the measured signal.

While the traditional way of measuring the impedance curve is point-by-point, i.e. by measuring the response to each individual sinusoidal perturbation with a frequency ω, some novel approaches have been developed based on the simultaneous imposition of a set of various sinusoidal harmonics, or noise, or a small-amplitude potential step, with subsequent Fourier and Laplace data analysis. The self-consistency of the measured spectra is tested with the use of the Kramers–Kronig transformations, whose violation testifies in favor of a non-steady-state character of the studied system (say, in corrosion).

The total impedance can be written in concise form as

$$Z(\omega) = \mathrm{Re}(Z) - i \times \mathrm{Im}(Z) \tag{15.1}$$

where $\mathrm{Re}(Z) \equiv Z'$ and $\mathrm{Im}(Z) \equiv Z''$ are the *real* and the *imaginary* parts of the impedance, respectively (sometimes called *resistance* and *reactance*, respectively), and $i \equiv \sqrt{-1}$ is the imaginary unit. It follows that the absolute value of the impedance vector (also known as the *impedance modulus*) is given by

$$|Z(\omega)| = [(\mathrm{Re}(Z))^2 + (\mathrm{Im}(Z))^2]^{1/2} \tag{15.2}$$

When a sinusoidal voltage signal

$$V(t) = V_{\mathrm{m}} \sin(\omega t) \tag{15.3}$$

is applied across the interphase (V_{m} is the voltage amplitude), the result is a sinusoidal current signal of the same frequency but displaced somewhat in time,

$$I(t) = I_{\mathrm{m}} \sin(\omega t + \phi) \tag{15.4}$$

namely, having a *phase shift* ϕ. Here we use the current I, instead of the current density j. The phase angle may be defined as

$$\tan(\phi) = \frac{\mathrm{Im}(Z)}{\mathrm{Re}(Z)} = \frac{1}{\omega RC} \tag{15.5}$$

and the real and imaginary parts as

$$\mathrm{Re}(Z) = |Z| \cos(\phi) \tag{15.6}$$

$$\mathrm{Im}(Z) = |Z| \sin(\phi) \tag{15.7}$$

The value $|Z|$ has units of resistance; it is the length of a vector obtained by addition of two perpendicular vectors, R and $1/\omega C$.

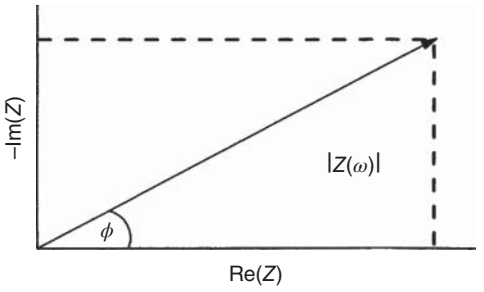

Figure 15.1 Vector representation of the impedance $Z(\omega)$ in the complex plane.

The AC analog to Ohm's law ($R = V/I$) is

$$Z(\omega) \equiv V(t)/I(\mathrm{t}) \tag{15.8}$$

Like resistance, impedance is a measure of the ability of a circuit to resist the flow of electric current.

In Figure 15.1 we can see the relations of the phase angle and the modulus to the real and imaginary components of the impedance.

For an ideally *polarizable* interphase with negligible solution resistance, the phase angle is −90°. For an ideally *nonpolarizable* interphase the phase angle is zero. Real systems do not behave ideally, of course. The actual phase angle will, therefore, be somewhere in between, and it will depend on frequency in most cases.

For a circuit containing both capacitors and resistors, the ratio between the applied voltage signal and the resulting current signal is the impedance $Z(\omega)$, which is a function of frequency. The impedance of a pure *resistor* is simply its resistance R, while the impedance of a pure *capacitor* is given by

$$Z_{\mathrm{C}} = -\frac{i}{\omega C} \tag{15.9}$$

For a capacitor and a resistor in *series* one has

$$Z(\omega) = R_{\mathrm{S}} - i/\omega C_{\mathrm{dl}} \tag{15.10}$$

while for a capacitor and resistor in *parallel* the impedance is given by

$$\frac{1}{Z(\omega)} = \frac{1}{R_{\mathrm{F}}} - \frac{\omega C_{\mathrm{dl}}}{i} \tag{15.11}$$

It is convenient to display the results of EIS in the *complex-plane impedance* representation. The x-axis on this plot is Re(Z), which is the Ohmic resistance, and the y-axis is −Im(Z), which, in the present case, is the capacitive impedance $-i/\omega C$. This is shown in Figure 15.2, which is a vector representation of $|Z|$ for both the series and parallel combinations.

As the frequency is *increased*, the capacitive impedance decreases, while the resistive impedance is unchanged. In the *series R–C circuit*, this makes the circuit behave more and more like a pure *resistor*, causing a decrease in the phase angle, as seen in Figure 15.2a. The impedance in this case is given by $Z = R - \mathrm{i}/\omega C$. The Nyquist graph in this case consists of a straight line perpendicular to the real axis, while the Bode modulus graph (not shown here) contains one breakpoint (following slope = −1). This point corresponds to the system characteristic frequency

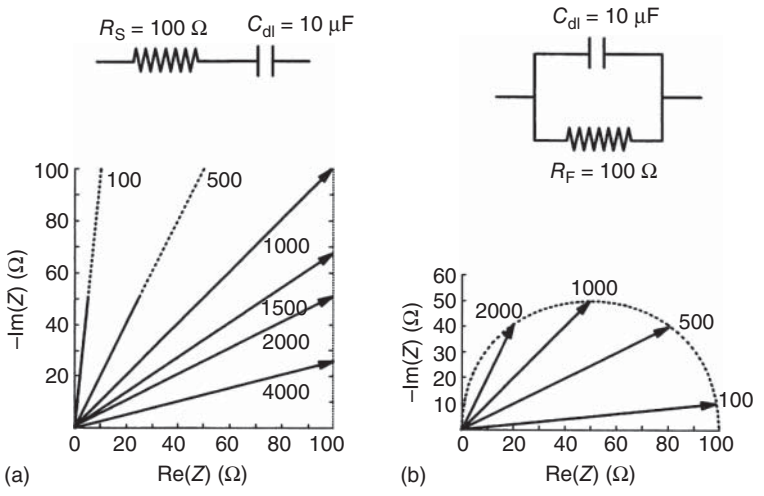

Figure 15.2 Vector representation of the impedance of (a) series and (b) parallel combination of a capacitor and a resistor, showing the variation of ϕ with ω (expressed in radians per second). The ends of the arrows show the absolute values of the vectors, except at the two lowest frequencies in the series combination.

$\omega = 1/RC$, or a time constant $\tau = RC$. The Bode phase-angle graph changes from 90° at low frequencies to 0° at high frequencies.

A *parallel R–C circuit* makes the circuit behave more and more like a *capacitor*, causing an increase in phase angle, as shown in Figure 15.2b. In this case, the total admittance is $Y(i\omega) = 1/R + i\omega C$, so that

$$Z(\omega) = \frac{1}{1/R + i\omega C} = \frac{R}{1 + i\omega RC} = \frac{R}{1 + \omega^2 R^2 C^2} - \frac{i\omega R^2 C}{1 + \omega^2 R^2 C^2} \qquad (15.12)$$

There are two impedance limits in this case: ($\omega = 0$, $Z = R$) and ($\omega \to \infty$, $Z = 0$). The Nyquist diagram will show a semicircle of radius $R/2$ with its center on the real axis, the frequency at the semicircle maximum being $\omega = 1/RC$. The circuit's characteristic breakpoint frequency (inverse of the characteristic time constant), as observed in the Bode modulus plot (not shown here), is the same as for the series R–C circuit. The complex plane admittance plot will show a straight line parallel to the imaginary axis, which is similar to the complex-plane impedance plot for the series R–C circuit.

Consider now a more realistic situation, in which both the series and the parallel resistance must be taken into account. The Randles equivalent circuit (see also Chapters 1 and 4) and the corresponding complex-plane impedance plot are shown in Figure 15.3. Let us derive the mathematical expression for the impedance applicable to this circuit, as a function of the angular frequency, ω:

$$Z(\omega) = R_S + \frac{1}{1/R_F - \omega C_{dl}/i} = R_S + \frac{R_F}{1 + i\,\omega C_{dl} R_F} \qquad (15.13)$$

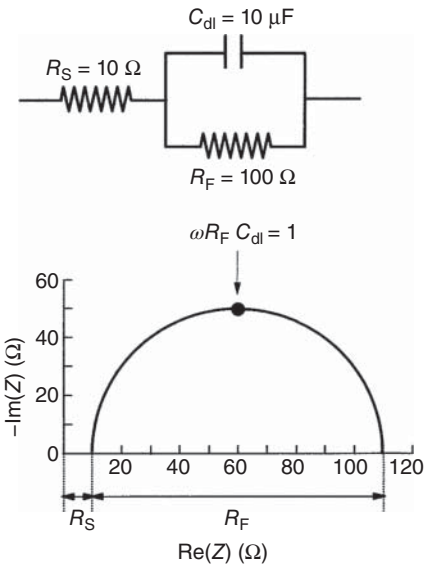

Figure 15.3 Complex-plane representation of the impedance of an interphase. The equivalent circuit in this case is known as the Randles equivalent circuit.

The following simple manipulation allows us to separate the real from the imaginary part of the impedance:

$$Z(\omega) = R_S + \left[\frac{R_F}{1 + i\omega C_{dl} R_F}\right] \times \left[\frac{1 - i\omega C_{dl} R_F}{1 - i\omega C_{dl} R_F}\right] \tag{15.14}$$

which leads to the expression

$$Z(\omega) = R_S + \frac{R_F}{1 + (\omega C_{dl} R_F)^2} - i \times \frac{\omega C_{dl} R_F}{1 + (\omega C_{dl} R_F)^2} \tag{15.15}$$

The result is a semicircle having a diameter equal to R_F, with its center on the x-axis and displaced from the origin of coordinates by $R_S + R_F/2$. Each point on the semicircle in Figure 15.3 represents a measurement at a given frequency. At the limit of high frequencies, the faradaic resistance is effectively shorted out by the double-layer capacitance, leaving the solution resistance R_S as the only measured quantity. At the limit of low frequency the opposite occurs: the capacitive impedance becomes very high, and one measures only the sum of the two resistors, $R_S + R_F$, in series. The same conclusion can be reached by substituting either high or low angular frequency in Eq. (15.13).

The double-layer capacitance can be obtained from this plot, since the maximum on the semicircle satisfies the equation

$$R_F \times C_{dl} \times \omega_{max} = 1 \tag{15.16}$$

When one studies an (almost) ideally polarizable interphase, such as the mercury electrode in pure deaerated acids, the equivalent circuit is a resistor R_S, and a capacitor C_{dl} in series. The high accuracy and resolution offered by modern instrumentation allows measurement in such cases in very dilute solutions or in poorly conducting, nonaqueous media, which could not have been performed in the early days of studying the mercury/electrolyte interphase.

15.2 Graphical Representations

The measured impedance data can be displayed in a number of different forms, each having its own coordinates:

(1) Plot of data for various frequencies as a set of points in the complex-impedance plane, $\mathrm{Re}(Z)$ and $-\mathrm{Im}(Z)$ being the x and y axes, respectively. This graph presentation is known as the complex-plane plot, *Nyquist* diagram, or Argand plot.
A *resistor* will be represented on the Nyquist plot by a single point on the real axis of this diagram; the impedance of a resistor is independent of frequency and has no imaginary component. With only a real impedance component, the current through a resistor stays in phase with the voltage across the resistor.
The impedance of an *inductor* increases as frequency increases. An inductor will be represented on the Nyquist plot by a vertical line coinciding with the imaginary axis. Since inductors have only an imaginary impedance component, the current through an inductor is phase-shifted −90° with respect to the voltage.
The impedance versus frequency behavior of a *capacitor* is opposite to that of an inductor; a capacitor's impedance decreases as the frequency is raised. Thus, a capacitor will be represented on the Nyquist plot by a vertical line coinciding with the imaginary axis. Capacitors also have only an imaginary impedance component. The current through a capacitor is phase-shifted −90° with respect to the voltage.
An *ideally polarizable* electrode behaves as an ideal capacitor because there is no charge transfer across the solution/electrode interphase. The impedance of an ideally polarizable electrode produces a straight line, perpendicular to the real axis of the Nyquist diagram.
The Nyquist plot has been commonly used in the electrochemical literature because it allows for an easy relation to the electrical model. However, the frequency itself is typically not shown on the Nyquist diagram, and this is one of the disadvantages of this form of presentation. This is sometimes corrected by marking the frequencies at which specific measurements were taken on the semicircle. *The diameter of the semicircle is equal to the faradaic resistance, and is independent of the capacitance*. As a result, plots measured for a fixed value of R_F but different values of C_{dl} cannot be distinguished in this type of presentation, even though corresponding points on the semicircle have been measured at different frequencies.
(2) Plots of $\log |Z|$ and ϕ versus $\log f$. These presentations are known as the *Bode modulus plot* and the *Bode phase-angle plot*, respectively. On the Bode modulus plot, a resistor will be represented by a horizontal line, whereas a capacitor will be represented by a line with a slope = −1. The Bode plots contain all the necessary information. That is why they are nowadays probably the most commonly used graphical presentations.
(3) Plots of $\mathrm{Re}(Z)$ and $\mathrm{Im}(Z)$ versus frequency (usually, $\log f$). This presentation is rarely used.

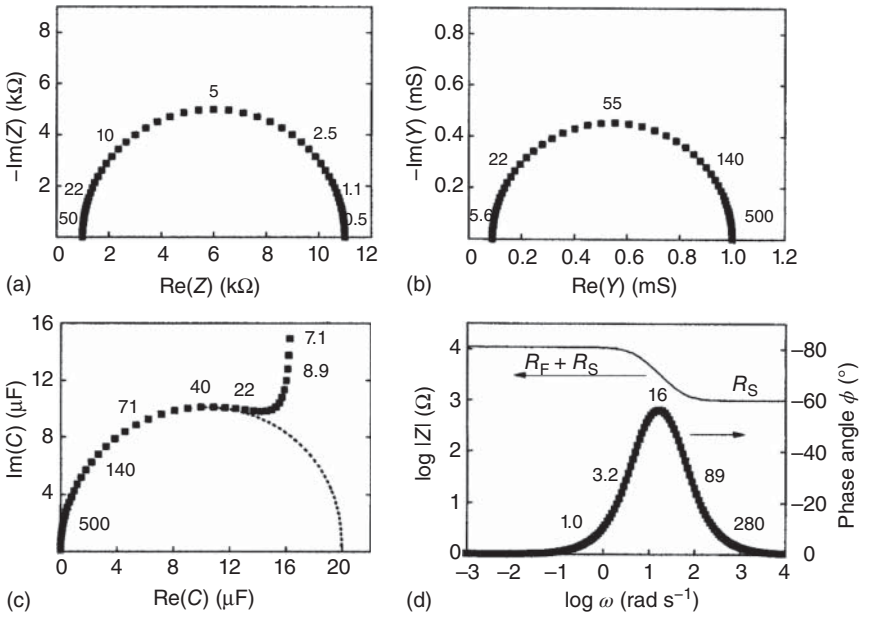

Figure 15.4 Comparison of (a) complex-plane impedance, (b) complex-plane admittance, (c) complex-plane capacitance, and (d) Bode modulus and phase angle plots for the same equivalent circuit. $R_F = 10\,k\Omega$, $R_S = 1\,k\Omega$, $C_{dl} = 20\,\mu F$. Values of ω (rad s^{-1}), at which some of the points were calculated, are shown.

(4) Recalculation of the impedance data to yield various other complex characteristics, most frequently the *admittance* $Y \equiv 1/Z$, and the complex capacitance $C \equiv Y/i\omega$. For the complex-plane admittance plot (see Figure 15.4b), the real and the imaginary parts of the admittance are defined as

$$\mathrm{Re}(Y) = \frac{\mathrm{Re}(Z)}{(|Z|)^2} \tag{15.17}$$

and

$$\mathrm{Im}(Y) = \frac{\mathrm{Im}(Z)}{(|Z|)^2} \tag{15.18}$$

For the complex-plane capacitance form (see Figure 15.4c)

$$\mathrm{Re}(C) = \frac{\mathrm{Im}(Z)}{(|Z|)^2}\frac{1}{\omega} \tag{15.19}$$

and

$$\mathrm{Im(C)} = \frac{\mathrm{Re(Z)}}{(|\mathrm{Z}|)^2}\frac{1}{\omega} \tag{15.20}$$

In Figure 15.4 above, different forms of presenting the response of the same circuit are compared. The values of the components constituting the equivalent circuit were chosen as $R_F = 10\,k\Omega$, $R_S = 1\,k\Omega$, and $C_{dl} = 20\,\mu F$. Each way of presentation has its own advantages and disadvantages. From the impedance plot, R_F and R_S can be read directly, and the double-layer capacitance can

be calculated, employing Eq. (15.16). The relevant time constant in this case is $\tau = R_F \times C_{dl} = 0.20\,s$; hence, $\omega = 5\,rad\,s^{-1} = 0.80\,Hz$. The complex-plane admittance plot yields the values of $1/R_F$ and $1/R_S$, but it is rarely used.

On the complex-plane capacitance plot, the semicircle results from the series combination of R_S and C_{dl} while the intercept with the real axis yields the value of C_{dl}. The vertical line is due to the parallel combination of R_F and C_{dl}. While the physical meanings of complex impedance and complex admittance are clear, that of the complex capacitance is questionable. Nevertheless, presenting the data as in Figure 15.4c has some merit, because the numerical value of C_{dl} is given directly as the diameter of the semicircle.

Plotting the same data in the Bode-type representation, one notes two points:

(a) Although the values of the two resistors are easily discerned, there is no region in which the circuit behaves as a pure capacitor. The slope never reaches a value of −1 in this figure, and ϕ never comes close to −90°, which one would expect for a pure capacitor.
(b) The phase angle is a more sensitive test of the capacitive or resistive behavior of the system than the plot of $\log|Z(\omega)|$ versus $\log(\omega)$. The detailed shape of these curves depends, of course, on the numerical values chosen for the various circuit elements. Had we used a value of $R_S = 10\,\Omega$ instead of 1 kΩ, the two horizontal lines in Figure 15.4d would have been much farther apart, and an (almost) pure capacitive behavior would have been observed in the intermediate region.

It would seem then that the complex-plane impedance plot is the best way of presenting the data, if one is mainly interested in the value R_F and its variation with time or potential. The complex-plane capacitance plot, on the other hand, brings out more directly the value of the capacitance and its variation with the different parameters of the experiment.

It should be remembered that the curves shown in Figure 15.4 are all simulated and therefore "ideal," in the sense that they follow exactly the equations used for the assumed equivalent circuit and the numerical values of its components. When conducting an experiment, the points are always scattered as a result of experimental error. Also, the frequency range over which reliable data can be collected does not necessarily correspond to the time constant of the system studied. Thus, for the case shown in Figure 15.4a, the semicircle can be constructed from measurements in the range of $1 \le \omega \le 20\,rad\,s^{-1}$. In Figure 15.4b one would have to use data in the range of about $10 \le \omega \le 200\,rad\,s^{-1}$ to evaluate the numerical values of the circuit elements. From the Bode magnitude plots, R_S can be evaluated from high-frequency measurements ($\omega \ge 100\,rad\,s^{-1}$), while R_F can be obtained from low-frequency data ($\omega \le 1\,rad\,s^{-1}$). The capacitance can be obtained *approximately* as $C_{dl} = 1/(\omega\,|Z|)$ at the inflection point (which coincides with the maximum on the Bode angle plot), but this is correct only if $\phi = -90°$, that is, if the circuit behaved as a capacitor at this frequency. In the present example, $\phi_{max} = -58°$ and the value of C_{dl} calculated in this manner is 18.4 μF, compared to the value of 20 μF used to calculate the curves.

When impedance spectroscopy was introduced to electrochemistry, there was some argument in the literature as to the best method of displaying EIS data.

Nowadays, the software provided with most commercial instruments allows us to display the data in all the ways shown in Figure 15.4 and choose the representation that best suits the particular purpose, making the above argument obsolete.

15.3 The Effect of Diffusion Limitation – The Warburg Impedance

So far in this chapter we have discussed only equivalent circuits that correspond to charge transfer, namely, the situation in which the faradaic resistance R_F is high and diffusion limitation is negligible. We might note in passing that EIS is inherently a *small-amplitude technique*, in which the AC component of the *j/E* relationship is in the linear region. This is most readily realized by maintaining the system at its OCP and applying a low-amplitude perturbation. However, the response to a small perturbation can be linear, even if the system is in the nonlinear region. The faradaic resistance measured by EIS is the *differential* resistance, defined as

$$R_F \equiv (\partial\eta/\partial j)_\mu \tag{15.21}$$

In the high-overpotential region, j is an exponential function of the overpotential; hence, the differential faradaic resistance also depends exponentially on potential:

$$\eta = b \ \log j/j_0 \tag{15.22}$$

Combining the last two equations, one has, for the high-overpotential region,

$$R_F = \frac{b}{j} \tag{15.23}$$

In the low-overpotential region, where the current is linearly related to the overpotential,

$$\frac{j}{j_0} = \frac{nF}{RT}\eta \tag{15.24}$$

Hence, in this region the faradaic resistance is given by

$$R_F = \frac{\eta}{j} = \frac{1}{j_0}\frac{RT}{nF} \tag{15.25}$$

It is very important to note the difference between the two expressions for the differential faradaic resistance, given in Eqs. (15.23) and (15.25). At high overpotential, R_F is inversely proportional to the current density, but it yields no information concerning the exchange current density (and, hence, of the heterogeneous rate constant). For example, it is well known that j_0 for electrodeposition of Cu is about 3 orders of magnitude higher than that for Ni. Nevertheless, if EIS is used to measure R_F at the same current density, the same value will be observed in both cases, unless the Tafel slope is different. However, this change could be a factor of 2 or 3 at most, while the exchange current density could vary over several orders of magnitude. In contrast, when EIS is applied to a system at its

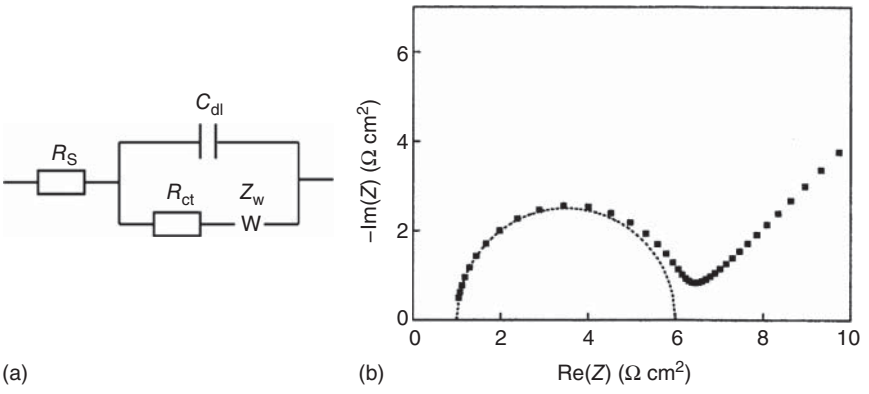

Figure 15.5 (a) Modified Randles equivalent circuit due to diffusion limitation. (b) Complex-plane impedance plot for an equivalent circuit with diffusion limitation at low frequencies. The values chosen for this simulation were $R_F = 5\,\Omega\,cm^2$, $R_S = 1\,\Omega\,cm^2$, $C_{dl} = 20\,\mu F\,cm^{-2}$, $c_{b,Ox} = c_{b,Red} = 10\,mM$, $D_{Ox} = D_{Red} = 1 \times 10^{-5}\,cm^2\,s^{-1}$, $\sigma = 12\,\Omega\,cm^2\,s^{-1/2}$, $j_0 = 5\,mA\,cm^{-2}$, $k_{s,h} = 5 \times 10^{-3}\,cm\,s^{-1}$. Frequency range: $1 \times 10^{-3} \leq \omega \leq 1 \times 10^3\,rad\,s^{-1}$.

reversible potential, or at the OCP, Eq. (15.25) is applicable, and the value of j_0 can be obtained directly.

Turning now to the case in which diffusion control must be considered (e.g. under conditions of concentration polarization, when surface layer is formed, or when top coating is present), the equivalent circuit takes the form shown in Figure 15.5a, in which the symbol "W" represents the so-called *Warburg impedance*, which accounts for diffusion limitation. The diffusion equations have been solved for the low-amplitude sine wave perturbation. It is found that the Warburg impedance is given by

$$Z_W = \frac{\sigma}{\omega^{1/2}} - i\frac{\sigma}{\omega^{1/2}} \tag{15.26}$$

where the parameter σ, also known as the Warburg impedance coefficient, is defined as

$$\sigma = \frac{RT}{(nF)^2}\frac{1}{\sqrt{2}}\left[\frac{1}{c_{b,Ox} \times D_{Ox}^{1/2}} + \frac{1}{c_{b,Red} \times D_{Red}^{1/2}}\right] \tag{15.27}$$

This equation can be simplified if it is assumed that the two diffusion coefficients are equal, and the bulk concentrations of the oxidized and the reduced species are also equal, yielding

$$\sigma = \frac{RT}{(nF)^2}\frac{2^{1/2}}{c_b \times D^{1/2}} \tag{15.28}$$

If the two concentrations differ widely, Eq. (15.27) shows that the lower concentration determines the value of σ.

One should note that the real and the imaginary parts of the Warburg impedance in Eq. (15.26) depend on frequency in the same way. Therefore, the phase shift generated by the Warburg impedance is independent of frequency.

Plotted in the complex-plane impedance format, this leads to a straight line with a slope of unity (a phase shift of 45°), as shown in Figure 15.5.

Equations (15.26)–(15.28) were derived for conditions of semi-infinite linear diffusion. Thus, measurements should be conducted in quiescent solutions. In addition, if there is a thin film on the surface through which diffusion occurs, such as the solid electrolyte interphase (SEI) formed in some nonaqueous batteries, the condition of semi-infinite linear diffusion no longer applies, and the part corresponding to diffusion in Figure 15.5 will be different.

We note that the Warburg impedance, which is proportional to $\omega^{-1/2}$, is in series with the faradaic resistance, R_F, as seen in Figure 15.5. At high frequencies, one obtains the usual semicircle, whereas the Warburg impedance becomes predominant at low frequencies. The frequency at which the transition occurs depends on the concentrations of reactants and products (which determine the value of σ), on the exchange current density, and on the overpotential, which determine the value of the faradaic resistance, R_F.

Four complex-plane impedance plots, calculated for the concentrations of 100, 10, 1, and 0.1 mM, respectively, are shown in Figure 15.6a–d. Note that R_F, which is proportional to $1/j_0$, also depends on concentration; therefore, the scale of both Im(Z) and Re(Z) must be changed from Figure 15.6a–d. In calculating the curves of this figure, it was assumed that j_0 is a linear function of concentration, which is not always the case. At the highest concentration shown here, a semicircle characteristic of a charge-transfer-limited process is clearly seen, with diffusion limitation becoming important only at low frequencies. As the concentration is decreased, diffusion limitation becomes gradually more important. In a 1 mM solution, the initial part of the semicircle is barely seen, while in a 0.1 mM solution the process is mostly diffusion controlled. The values of R_F chosen here correspond to a moderately slow reaction, having a standard heterogeneous rate constant of $k_{s,h} = 2.7 \times 10^{-3}$ cm s^{-1}.

It is important to realize that the plots we have shown above are all based on simulated data and serve the purpose of illustrating the principles involved. The results of real experiments are rarely as simple and easy to interpret. This is caused by two types of factors: (i) the use of EIS is straightforward only when the behavior is simple and can be modeled by an equivalent circuit that involves just a few adjustable parameters, and (ii) the real picture found experimentally is rarely as simple as that shown by simulation. When complex shapes of the impedance spectrum are observed, one must develop a physical model and choose a corresponding equivalent circuit that can simulate the observed results. However, when fitting the model requires many adjustable parameters, the validity of the model becomes less reliable. In such cases, an independent experiment, such as considering the dependence of different parts of the spectrum on factors such as potential or current density, the concentration of the electroactive components, as well as the supporting electrolyte, can be useful. However, this approach weakens the usefulness of EIS in the study of electrode kinetics – rather than employing this technique to evaluate the physical model, one may end up using an assumed model to explain the complex impedance spectrum.

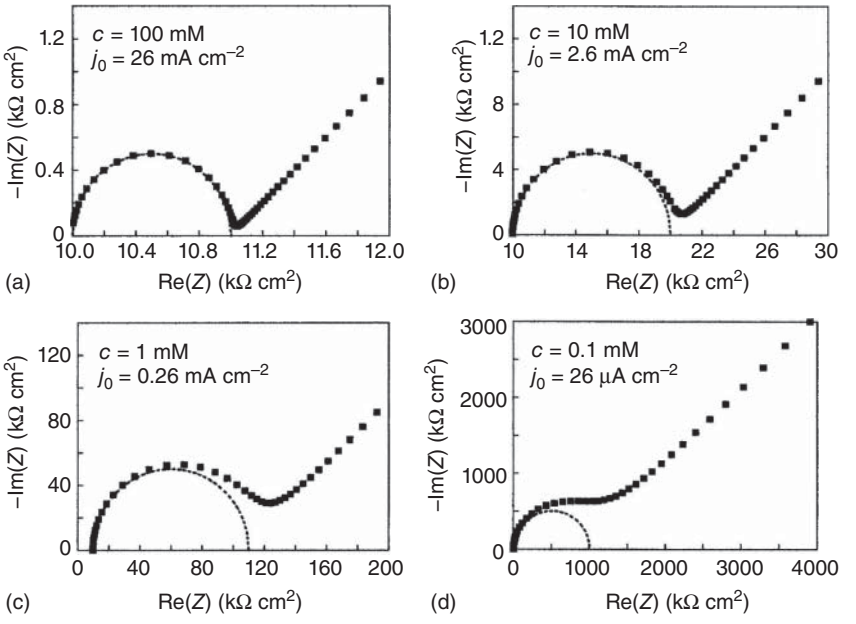

Figure 15.6 Complex-plane impedance plots showing the gradual change from charge-transfer to mass-transport control with decreasing concentration. $R_s = 10\,\Omega\,cm^2$, $C_{dl} = 20\,\mu F\,cm^{-2}$, $j_0 = 26, 2.6, 0.26, 0.026\,mA\,cm^{-2}$ for (a), (b), (c), and (d), respectively. Frequency range: $1 \times 10^{-3} \leq \omega \leq 1 \times 10^3$ rad s^{-1}.

15.4 Advantages, Disadvantages, and Applications of EIS

The advantages of EIS include the following: (i) The absence of any significant perturbation to the system. (ii) Its applicability to the assessment of low-conductivity media such as polymers. (iii) The existence of a frequency component that may provide mechanistic information. Furthermore, EIS may be able to distinguish between two or more electrochemical reactions taking place. (iv) EIS can test components within an assembled device using the device's own electrodes. (v) EIS can identify diffusion-limited reactions, e.g. diffusion through a passive film.

However, EIS also has some significant drawbacks: (i) At low frequencies, where underfilm corrosion reactions, for example, are probed, experimental difficulties and time constraints can complicate precise determination of the charge-transfer resistance R_{ct} and the double-layer capacitance C_{dl}. (ii) The Warburg impedance may exhibit a masking effect. (iii) Inductive loops or new time constants are sometimes observed at low frequency. Such inductive loops are generally ascribed to the existence of relaxation processes of adsorbed species (e.g. relaxation of coverage due an adsorbed intermediate), to surface area or salt film property modulation, etc. (iv) Owing to the long measurement time required, both the corrosion rate and corrosion potential can change during the experiment. (v) There has been no evidence that R_{ct} can be equated to R_p and be used in the Stern–Geary equation to calculate the underfilm corrosion rate.

(vi) In-depth mechanistic and kinetic information on the corroding interface can easily be overlooked in EIS by modeling the system with an oversimplified equivalent circuit.

EIS is a mature technique. It is one of the most widely employed techniques for studying the corrosion protection by paints and organic coatings, for predicting the lifetime of coating/metal systems, and for determining the effectiveness of corrosion inhibitors. It is also used to assess interfacial reactions; adsorption to and desorption from an electrode surface; chemical reactions coupled with faradaic processes; conducting polymers; electrochemical synthesis of materials; ions mobility in energy storage and conversion devices such as batteries, supercapacitors, and fuel cells; semiconductors; kinetics of electrocatalytic reactions; label-free detection sensors; etc.

Here, we give as an example the use of EIS for assessing the development of corrosion of ferromagnetic cobalt (in the forms of foil and e-beam deposit on silicon wafer), either bare or coated with an acrylic polymer, in 0.5 M NaCl electrolyte solution. The potential was maintained at the OCP during the experiment, with a superimposed perturbation of 20 mV for coated samples and 5 mV for bare samples. The frequency range was 20 mHz to 50 kHz. The most common equivalent circuit employed for polymer-coated systems is presented in Figure 15.7a. In this figure, R_f and C_f are the film (coating) resistance and capacitance. Diffusion processes are represented by the Warburg impedance Z_W, which can be related to blockage of oxygen diffusion paths by corrosion products. For a non-degraded polymer-coated metal system, before the interface becomes active, only the external circuit (R_S, R_f, and C_f) will be observed experimentally. With time, however, the inner circuit (R_{ct}, C_{dl}, and Z_W) may also become active, and this is the source of a second time constant. The appearance of the latter has been linked with system breakdown. The two time constants represent the film (τ_f) at higher frequencies and the metal (τ_m) at lower frequencies. In order to determine the rate of corrosion and, hence, the mass loss, the R_{ct} (or R_p) value needs to be detected. While in the simplest situation, R_{ct} and R_p may be equivalent, these values are not necessarily the same.

Figure 15.7b–d presents the EIS Bode and Nyquist plots for bare cobalt with increasing times of exposure to the electrolyte. The polarization resistance was measured as the difference between the two plateaus in the Bode modulus plot (Figure 15.7d). Similar values were obtained by measuring the diameter of the depressed semicircle in the Nyquist plot. Sweeps performed at times longer than 69 hours of immersion yielded spectra that could not be deconvolved for analysis. Such behavior may result from the significantly reduced volume of cobalt and the exposure of the silicon wafer beneath the cobalt film.

In the case of polymer-coated cobalt, EIS analysis could only be made after some immersion time, when the cobalt beneath the polymer was clearly exposed. This was reflected by the appearance of a second semicircle at low frequencies in the Nyquist plot. EIS analysis was also not possible after long immersion times, likely due to masking effects of diffusion through corrosion products, which had formed at the bottom of defects in the coating and/or exposure of the silicon substrate. Selected Bode and Nyquist plots for the coated samples are shown in Figure 15.7e,f.

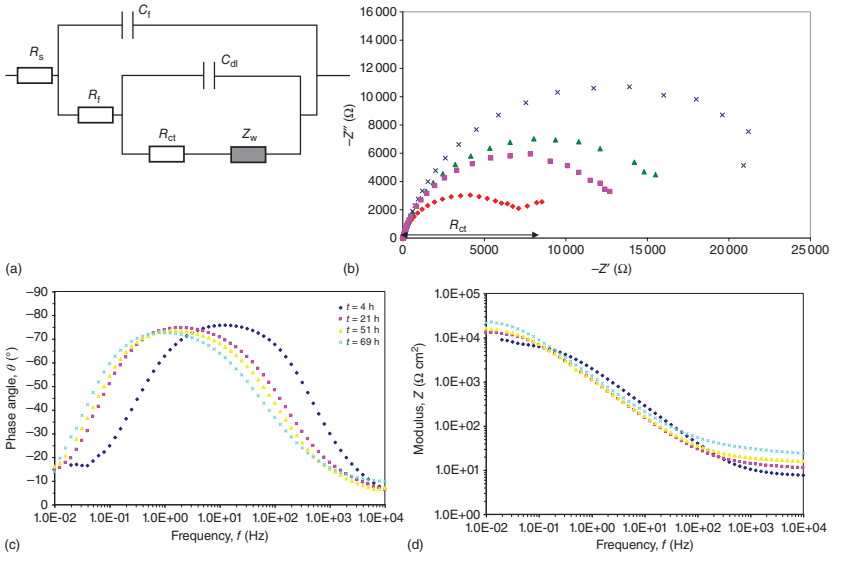

Figure 15.7 (a) The equivalent circuit frequently used to represent polymer-coated metals. In this figure, R_f and C_f are the coating resistance and capacitance, respectively. Source: Adapted from Mitton et al., *J. Electrochem. Soc*. **149** (2002) B265. Nyquist (b) and Bode (c,d) EIS plots of bare cobalt after 4, 21, 51, and 69 hours of immersion. Sweeps performed at times longer than 69 hours of immersion yielded spectra, which could not be deconvolved for analysis. (e,f) EIS Nyquist plots for polymer-coated cobalt after 6, 93, 169, and 302 hours of immersion. Only the data after 93 and 169 hours could be used for the determination of R_{ct}. Note the different scales of the Z' and Z'' axes in (e) and (f). Source: Adapted from Eliaz et al., *Mater. Technol*. **16** (2001) 90.

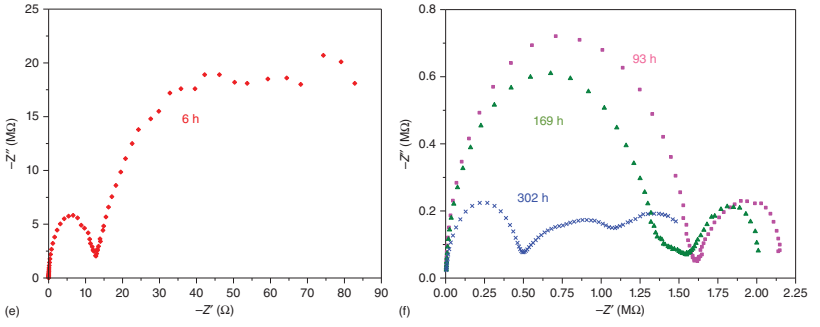

Figure 15.7 (*Continued*)

How can we determine the cumulative mass loss due to corrosion based on EIS measurements? First, the corrosion rate, CR (g cm^{-2} s^{-1}), should be determined:

$$\mathrm{CR} = \frac{a_\mathrm{m} \cdot j_\mathrm{corr}}{nF} \tag{15.29}$$

where a_m is the atomic mass of the corroding metal (g mol^{-1}), j_corr is the corrosion current density (A cm^{-2}), n the number of electrons transferred in the reaction (dimensionless), and F the Faraday constant (C mol^{-1}).
Substituting the Stern–Geary relation for j_corr,

$$\mathrm{CR} = \frac{a_\mathrm{m}}{nFAR_\mathrm{p}} \cdot \frac{b_\mathrm{a}|b_\mathrm{c}|}{2.3(b_\mathrm{a} + |b_\mathrm{c}|)} \tag{15.30}$$

where A is the exposed surface area (cm^2), R_p the polarization resistance (Ω cm^2), and b_a and b_c are the anodic (oxidation) and cathodic (reduction) Tafel slopes (V decade^{-1}).

The cumulative mass loss is thus

$$\Delta m = \int_{t_0}^{t_n} (\mathrm{CR}) A \, \mathrm{d}t \tag{15.31}$$

The capacitance of an organic coating, C_f, is an important measure of coating failure. It is defined by

$$C_\mathrm{f} = \frac{\varepsilon \varepsilon_0 A}{d} \tag{15.32}$$

where ε is the dielectric constant of the coating, ε_0 is the permittivity of free space (electric constant), A is the surface area of the working electrode exposed to the solution, and d is the coating thickness. Because most organic coatings are relatively thick, the coating capacitance is typically rather low, at around 1 nF cm^{-2}.

EIS can be used to monitor the absorption of water in organic coatings. The impedance from the Bode plot decreases when the coating absorbs water, but maintains a linear relationship with frequency. The slope does not change, and the phase angle remains −90°. Water has a higher dielectric constant (78.5 at 25 °C) than that of the typical organic coating (2–5). Therefore, the capacitance of the coating with absorbed water is higher than that of the dry coating (see Eq. (15.32)). The coating may also swell during this stage, thus resulting in decrease of the capacitance. Fortunately, because of the high dielectric constant of water, the effect of water absorption usually overwhelms the effect of swelling, and the capacitance increases. The initial effect of water absorption is to change the "value" of the capacitor, so the shape of the Nyquist plot does not change. The Brasher–Kingsbury equation provides a convenient estimate of water uptake in the coating:

$$\text{Volume fraction of } \mathrm{H_2O} = \frac{\log(C_{\mathrm{f,t}}/C_{\mathrm{f},0})}{\log \varepsilon_\mathrm{w}} \tag{15.33}$$

where $C_{\mathrm{f,t}}$ is the coating's capacitance at time t, $C_{\mathrm{f},0}$ is the initial coating's capacitance, and ε_w is the dielectric constant of water. The coating's capacitance can be easily measured at any time by fitting the equivalent circuit to the EIS data.

Further Reading

1 Lasia, A. (2014). *Electrochemical Impedance Spectroscopy and its Applications*. New York, USA: Springer-Verlag.
2 Bard, A.J., Inzelt, G., and Scholz, F. (ed.) (2012). *Electrochemical Dictionary*. Berlin Heidelberg: Springer-Verlag.
3 Orazem, M.E. and Tribollet, B. (2008). *Electrochemical Impedance Spectroscopy*. New York, USA: Wiley.
4 Mitton, D.B., Wallace, S.L., Cantini, N.J. et al. (2002). The correlation between substrate mass loss and electrochemical impedance spectroscopy data for a polymer-coated metal. *J. Electrochem. Soc.* 149: B265–B271.
5 Turgoose, S. and Cottis, R. (1999). *Electrochemical Impedance and Noise*. NACE International.
6 Bonora, P.L., Deflorian, F., and Fedrizzi, L. (1996). Electrochemical impedance spectroscopy as a tool for investigating underpaint corrosion. *Electrochim. Acta* 41: 1073–1082.
7 McIntyre, J.M. and Pham, H.Q. (1996). Electrochemical impedance spectroscopy: a tool for organic coatings optimizations. *Prog. Org. Coat.* 27: 201–207.
8 Mansfeld, F. (1995). Use of electrochemical impedance spectroscopy for the study of corrosion protection by polymer coatings. *J. Appl. Electrochem.* 25: 187–202.
9 Macdonald, J.R. (1987). *Impedance Spectroscopy: Emphasizing Solid Materials and Systems*. New York, USA: Wiley.
10 Brasher, D.M. and Kingsbury, A.H. (1954). Electrical measurements in the study of immersed paint coatings on metal. I. Comparison between capacitance and gravimetric methods of estimating water-uptake. *J. Appl. Chem.* 4: 62–72.
11 Randles, J.E.B. (1947). Kinetics of rapid electrode reactions. *Discuss. Faraday Soc.* 1: 11–19.